Large-scale topology and the default mode network in the mouse connectome

James M. Stafford[a,1], Benjamin R. Jarrett[b,1], Oscar Miranda-Dominguez[b], Brian D. Mills[b], Nicholas Cain[c], Stefan Mihalas[c], Garet P. Lahvis[b], K. Matthew Lattal[b], Suzanne H. Mitchell[b], Stephen V. David[b,d,e,f], John D. Fryer[g], Joel T. Nigg[b,d], and Damien A. Fair[b,d,e,2]

[a]Department of Biochemistry and Molecular Pharmacology, New York University School of Medicine, New York, NY 10016; Departments of [b]Behavioral Neuroscience and [d]Psychiatry and [e]Advanced Imaging Research Center, and [f]Oregon Hearing Research Center, Oregon Health & Science University, Portland, OR 97239; [c]Allen Institute for Brain Science, Seattle, WA 98103; and [g]Department of Neuroscience, Mayo Clinic College of Medicine, Jacksonville, FL 32224

Edited by Marcus E. Raichle, Washington University in St. Louis, St. Louis, MO, and approved November 4, 2014 (received for review March 6, 2014)

Noninvasive functional imaging holds great promise for serving as a translational bridge between human and animal models of various neurological and psychiatric disorders. However, despite a depth of knowledge of the cellular and molecular underpinnings of atypical processes in mouse models, little is known about the large-scale functional architecture measured by functional brain imaging, limiting translation to human conditions. Here, we provide a robust processing pipeline to generate high-resolution, whole-brain resting-state functional connectivity MRI (rs-fcMRI) images in the mouse. Using a mesoscale structural connectome (i.e., an anterograde tracer mapping of axonal projections across the mouse CNS), we show that rs-fcMRI in the mouse has strong structural underpinnings, validating our procedures. We next directly show that large-scale network properties previously identified in primates are present in rodents, although they differ in several ways. Last, we examine the existence of the so-called default mode network (DMN)—a distributed functional brain system identified in primates as being highly important for social cognition and overall brain function and atypically functionally connected across a multitude of disorders. We show the presence of a potential DMN in the mouse brain both structurally and functionally. Together, these studies confirm the presence of basic network properties and functional networks of high translational importance in structural and functional systems in the mouse brain. This work clears the way for an important bridge measurement between human and rodent models, enabling us to make stronger conclusions about how regionally specific cellular and molecular manipulations in mice relate back to humans.

connectivity | mouse | resting-state functional MRI | structural connectivity | default mode network

Understanding the functional architecture of brain systems in both typical and atypical populations has the potential to improve diagnosis, prevention, and treatment of various neurologic and mental illnesses. Human functional neuroimaging, because of its ease of use, noninvasive nature, and wide availability, has significantly advanced this goal. However, because functional brain imaging is an indirect measure of the underlying neuronal dynamics (1), a number of basic questions about the molecular and structural underpinnings of these functional signals needs to be answered before the full clinical promise of the technique can be realized. Insight into these underpinnings would be vastly enhanced by translation to rodent models, where rich methodology for studying high-throughput genetic, histological, and therapeutic conditions in a tightly controlled environment exists. Mouse models, in particular, are likely to contribute significantly to this end.

Efforts aimed at using mouse models to enrich findings obtained in humans with noninvasive imaging would benefit greatly from bridge measurements—measurements that can be obtained and compared directly between species, such as resting-state functional connectivity MRI (rs-fcMRI). Importantly, rs-fcMRI has provided invaluable insight into the large-scale topological organization of the human brain (2–4), how it relates to complex behaviors, and how it can be disrupted in disordered populations (5–8). In addition, rs-fcMRI is comparable across species, persists under light anesthesia, and allows for a broad view of intricate regional functional interactions without task inputs (9, 10). The capacity to image the murine brain with rs-fcMRI would effectively bridge clinical studies of human subjects with a vast array of techniques used to understand brain function with mouse models.

Although functional brain networks have been well-characterized in humans and to an increasing extent, macaques, a remaining question is whether there is conservation between species in large-scale topological features, such as the "Rich Club"—a system where highly connected brain regions (or hubs) also connect strongly with each other (11–13). Advances in rs-fcMRI and its computational evaluation have begun to shed some light on homology between brain networks in primates (14); however, there is a paucity of studies comparing primates with rodents. Despite evidence for intrinsic functional connectivity in rats (15–19) and to a lesser extent, mice (20–24), comparing large-scale network organization between mice and primates has proven difficult.

Of particular interest are prototypical functional networks, such as the default mode network (DMN). The DMN is a set of interconnected brain regions that were originally shown to decrease their level of activity in humans during goal-directed tasks (25, 26). These regions have subsequently been shown to be highly functionally connected in the human (27) and the macaque

Significance

Noninvasive brain imaging holds great promise for expanding our capabilities of treating human neurologic and psychiatric disorders. However, key limitations exist in human-only studies, and the ability to use animal models would greatly advance our understanding of human brain function. Mice offer sophisticated genetic and molecular methodology, but correlating these data to functional brain imaging in the mouse brain has remained a major hurdle. This study is the first, to our knowledge, to use whole-brain functional imaging to show large-scale functional architecture with structural correlates in the mouse. Perhaps more important is the finding of conservation in brain topology and default network among rodents and primates, thereby clearing the way for a bridge measurement between human and mouse models.

Author contributions: J.M.S., B.R.J., G.P.L., K.M.L., S.H.M., S.V.D., J.T.N., and D.A.F. designed research; B.R.J., O.M.-D., B.D.M., N.C., and S.M. performed research; O.M.-D., N.C., and S.M. contributed new reagents/analytic tools; J.M.S., B.R.J., O.M.-D., B.D.M., N.C., S.M., and D.A.F. analyzed data; and J.M.S., B.R.J., O.M.-D., B.D.M., G.P.L., K.M.L., S.H.M., S.V.D., J.D.F., J.T.N., and D.A.F. wrote the paper.

The authors declare no conflict of interest.

This article is a PNAS Direct Submission.

[1]J.M.S. and B.R.J. contributed equally to this work.

[2]To whom correspondence should be addressed. Email: faird@ohsu.edu.

This article contains supporting information online at www.pnas.org/lookup/suppl/doi:10.1073/pnas.1404346111/-/DCSupplemental.

NEUROSCIENCE

(9, 28). In addition, strength of functional connectivity in this system has been tied to several neurologic and psychiatric conditions, including Alzheimer's disease, Autism Spectrum Disorders, and Attention Deficit Hyperactivity Disorder (ADHD) among others (29). In rats, functional connectivity work has now revealed a potential default system surrogate (16); however, this network has yet to be revealed in the mouse, where rich genetic models, behavioral methodology, and the complete structural connectome exist. In addition, it is unclear whether this surrogate default system corresponds to direct connections of the underlying structural connectome.

This report fills this void by developing a high-resolution rs-fcMRI approach in mice, which combines with a brain-wide axonal projection mapping matrix [Allen Institute for Brain Science; connectivity.brain-map.org (30)] to (*i*) examine the structure–function relationships of rs-fcMRI in the mouse, (*ii*) directly test how well basic functional connectional topology is conserved between primates and the mouse, and (*iii*) considering this topology, identify whether a default mode-like network in mice exists.

Results

Strong Concordance Between Functional and Structural Connectivity. We first set out to validate our functional connectivity procedures by examining structure-to-function relationships in mouse connectivity by comparing our rs-fcMRI data with the full mouse brain axonal tracer-derived structural connectome. Qualitative maps of the functional and structural connections of selected seed regions are provided in Fig. 1. Selected seed regions reveal strong ties between the rs-fcMRI and the structural connectivity dataset in the primary motor cortex (10% connection density threshold) and dorsal anterior cingulate area seed regions (12% density threshold; also correspondence across species) (Fig. S1).

We next use quantitative analyses to examine how well functional connections are predicted by structural connections across all seeds. Using the structural data as the baseline, we generated a series of receiver operator characteristic curves (Fig. 2*A*) that began by examining the direct structure–function correspondence of the top 1% of structural connections. We followed this with a similar curve of the top 2% of structural connections and so on through 100% of the structural connections. Fig. 2*A* shows that the structural and functional data show strong correspondence across the series of curves, with the strongest correspondence having 78.26% sensitivity and 81.69% specificity for the top 1% of structural connections. This relationship highlights that functional connections, although not expected to be identical (*Discussion*), are tightly linked to underlying structural architecture, which is shown in other species (31–33). What is also clear from these plots is that the strongest structural connections (more than the top 10%) are more tightly related to the functional data. Importantly, compared with diffusion tensor imaging studies in humans and macaques (34), the axonal tracer structural data here have directionality. We found that the strongest correspondence was for the averaged axonal structural information (i.e., an average of the efferent and afferent projections between two nodes).

We note that, although the overall similarity between the connection matrices is strong, it is not perfect. Direct scatter plots and linear regression analysis comparing the correlative strength between functional and structural connections are highly significant ($P < 0.00001$) but modest in strength [Pearson's r (R) = 0.24] (Fig. 2*B*). As expected, using only the top 40% of structural connections

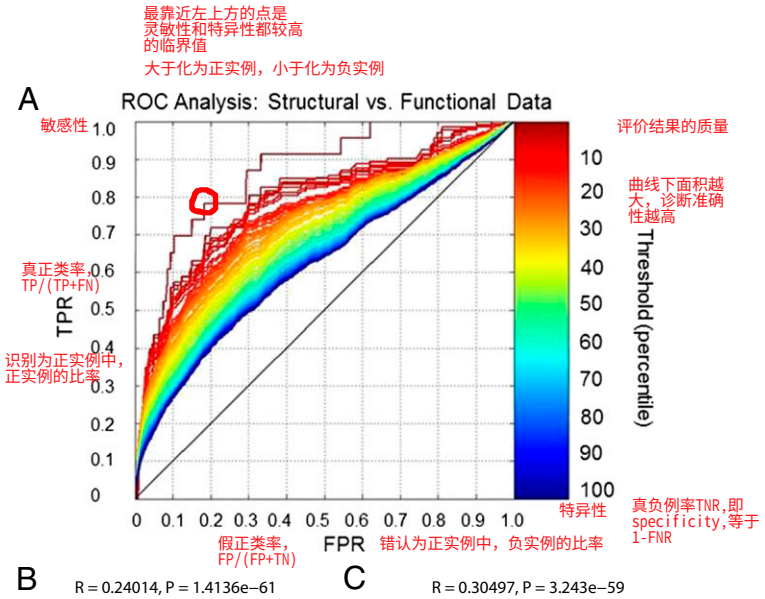

Fig. 2. Quantitative comparison of mouse functional and structural data. (*A*) Full matrix comparison of the structural data with the functional data using receiver operator characteristic (ROC) analysis (details in the text and *SI Methods*). (*B*) Structural weights (i.e., nonzero connections) from the structural matrix (*x* axis) were compared with the corresponding functional weights of the functional connectivity data (*y* axis). Structural connection weights were log-transformed. A modest Pearson's *r* value was observed with high significance ($P < 0.00001$). (*C*) The *r* value improved when the top 40% of the structural connections (i.e., top 10% of the total matrix) in *B* were considered (again with high significance; $P < 0.00001$). The structural data are presented on a lognormal scale because of the large range of connection strengths in the axonal structural data. TPR, true positive rate; FPR, false positive rate.

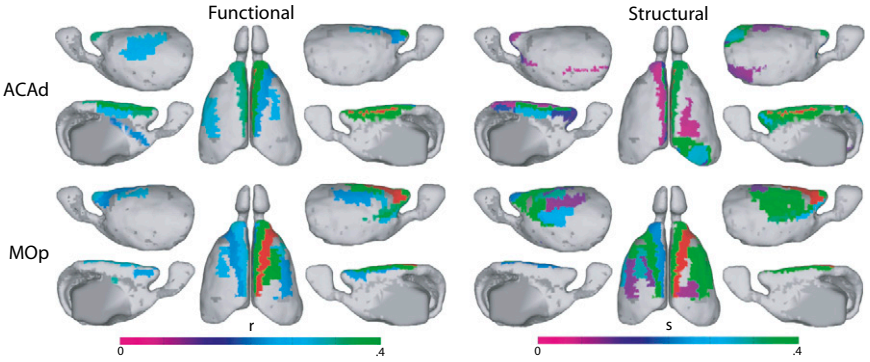

Fig. 1. Qualitative comparison of whole-brain mouse functional and structural data. Comparison of right primary motor cortex (MOp) and dorsal anterior cingulate (ACAd) seed regions. Note their strong similarities. The *r* label refers to correlation coefficient; *s* refers to the relative strength of the structural connections (30).

shown in Fig. 2*B* (i.e., top 10% of the total graph), the *R* values increased to 0.3 (Fig. 2*C*), showing stronger correlation when only examining the strongest structural connections.

Homology Between Mouse and Primate Functional Connectivity. Having shown reliable structure–function relationships, we next set out to determine whether features in the functional topology of the mouse connectome are shared across the species. Prior work has determined that many complex systems, including the brain, show a topological organization that supports a Rich Club system. Here, we expand on this concept and focus our efforts by determining the patterns in which a given region's number of connections (i.e., rich or poor) determines how that node will connect with the remaining regions of the system. Understanding such topological properties in rodents and how they compare with primates provides important context when attempting to examine a specified system (such as the default network) across species. It is an important consideration when evaluating the potential role, presence, and/or function of a potential default system in the mouse.

Functional topology was examined at three differing thresholds. We began by thresholding the functional connectivity matrix to match the density observed in the structural connectivity matrix, which has a density of 16.46%, followed by examinations at 10% and 20% connection densities. Fig. 3, *Upper Left* provides the degree and connectional distributions of the mouse functional connectome that rank orders nodes by their number of connections into 20 bins on each axis. The *z* axis then provides information on the percentage of existing connections from a given bin that connect to other nodes of varying degree. To test whether the observed connectional distribution differs significantly from what would be expected by chance (35), we generated 10,000 random connectivity matrices that preserved the degree distribution of the mouse connectome (Fig. 3, *Upper Center*). These two distributions were used to fit the data to their respective distribution functions, f_A (mouse) and f_B (random), as shown in Fig. 3, *Lower* (*SI Methods*). Simple subtraction of the data and its corresponding random realizations (Fig. 3, *Right*) shows qualitatively that the observed distributions are different from what are expected by chance (i.e., regions of high degree tend to connect with each other at a greater rate than would be expected by chance). Direct comparisons of these distributions (Fig. S2) were first measured with the discriminative function (*D*), which assumes that the mouse connectivity distribution is similar to the test distribution if *D* peaks at 0.5 (also represented by *D**, the discriminant function for the null hypothesis). Calculating the cumulative distributions (*F*s), shown in Fig. S2, allows direct comparison with the Kolmogrov–Smirnov test, because they are univariate distributions (35) (details in *SI Methods*). The combination of *D* and *F* measures deviating from 0.5 (Fig. S2*A*) and the fact that the distances between the two distributions (*d*s) are significantly different ($P < 0.0001$) show that the organization of the system in the mouse is significantly deviant from random chance. Highly connected regions tend to connect with themselves at a level greater than would be expected by chance. This finding would be similar to prior work, which has shown the presence of the Rich Club in other model systems (12, 36, 37) using a more tradition coefficient measure (Figs. S3, structural connectomes, and S4). For reference, node degrees for all regions are presented in Table S1 and as a surface map in Fig. S5.

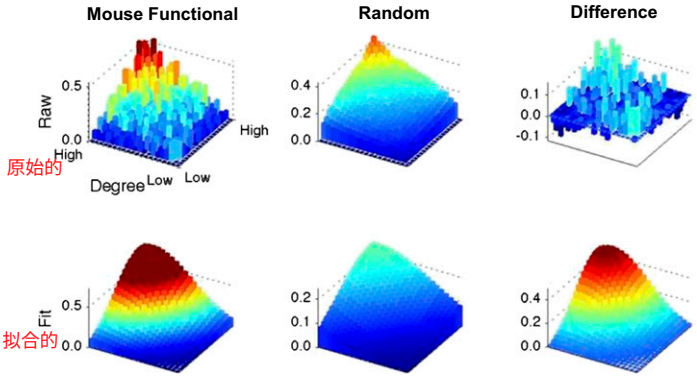

Fig. 3. Rank–rank distribution and Rich Club topology of the mouse's functional connectome. *Upper Left* shows the rank–rank distribution of the functional connections of the mouse connectome. *Lower Left* shows its fit to a bivariate distribution (details in the text and *SI Methods*). (*Center*) To determine if this topology is unique relative to what would be expected by chance, we generated a test distribution using the average of 10,000 random copies of the mouse connectome where the degree distribution was preserved. (*Right*) The functional and test distributions were compared by simple subtraction as shown.

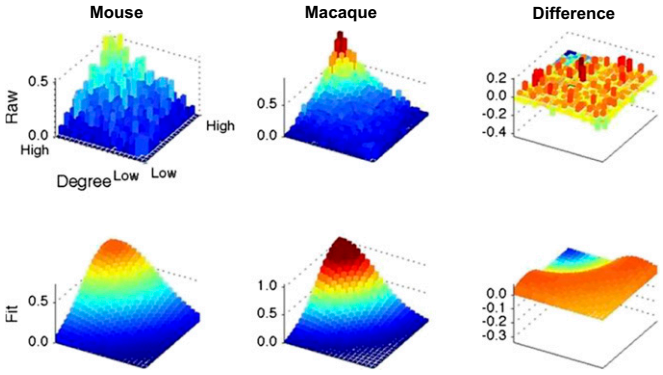

Fig. 4. Comparison between the mouse and macaque connectomes. Rank–rank distributions were compared between the mouse and macaque functional data using the same methodology as in Fig. 3.

Next, we applied this approach to assess homology in network topology between mice and primates. Comparisons of the mouse functional connectivity matrix were made using a density connection of 16.46% (i.e., density of the structural connectome) (*Methods*), with the corresponding functional data from macaques and humans at the same connection density. Again, this analysis was conducted at 10% and 20% connection densities as well (Figs. S6 and S7).

Fig. 4 shows how this connectional distribution compares with the macaque at a 16.46% connection density. Here, we see a similar overall distribution with some caveats. Notably, highly connected nodes seem to be more strongly connected to each other in the macaque relative to the rodent. In contrast, in the rodent, highly connected nodes tend to connect more often to other nodes that may have a moderate node degree. Importantly, the distributions of the connectional topology between the species were, indeed, significantly different ($P < 0.0001$), which was measured with the Kolmogrov–Smirnov test (Fig. S2*B*).

Connectional topology was then compared between the mouse and human datasets (Fig. 5). Similar trends as those of the macaque were identified ($P < 0.0001$) (Fig. S2*C*), with the main finding that highly connected nodes are similarly more connected to each other in the human than the rodent. In addition, highly connected nodes in the mouse tend to connect more often to other nodes that may have a moderate node degree. Last, in the human, not only do regions that have high degrees preferentially connect to nodes that also have high degrees, but nodes of any rank tended to connect to other nodes of similar rank. In other words, in humans, most of the connections are among bins with the same connection density (i.e., along the diagonal). Overall, these data suggest that, although the overall topology of the mouse shares features observed in primates, there are unique and likely important differences between the species.

Connectivity in the DMN. Understanding both some similarities and differences in the large-scale topology of the mouse from the prior

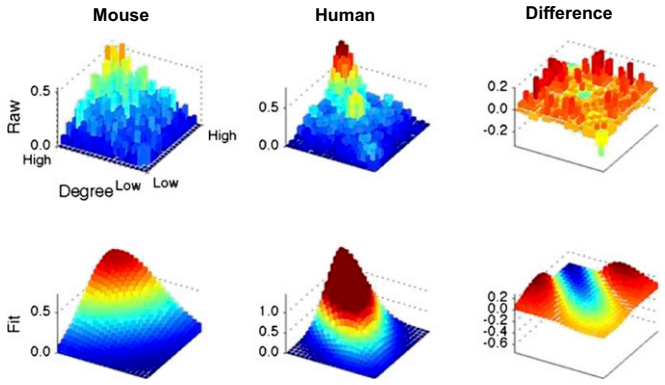

Fig. 5. Comparison between the mouse and human connectomes. Comparison of rank–rank distributions of the mouse and human functional connectomes using the same methodology as Fig. 3.

analyses, we next sought to evaluate whether a presumptive DMN identified in primates is also present in the mouse by first identifying seed regions that would allow for such a comparison. Seed-based correlations were conducted in humans, macaques, and mice. The macaque area parcellation scheme was based on the works by Miranda-Dominguez et al. (14) and Paxinos et al. (38). This macaque area atlas was registered through surface registration to the human data as well (14), such that the same area atlas could be used for both human and macaque comparisons (14, 39) (*SI Methods*). In the mouse, the area atlas used for comparisons was based on the atlas provided by the Allen Institute for Brain Science (*SI Methods*). Seed regions were chosen based on their presumptive importance as a major hub in the default system and their cytoarchitectural homology between species. For humans and macaques, we initially chose the retrosplenial cortex (RSP; area 30), because prior work has reported a ventral subsystem of the DMN that includes this area (23, 40–42). The murine RSP was used as the seed region based on prior work in the rat (16). Of note in our murine parcellation scheme, the RSP is subdivided into three regions [lateral agranular (RSPagl), dorsal, and ventral]. Based on posterior midline orientation and similar cytoarchitecture to the primate, we chose to focus on the RSPagl in mice. Furthermore, the RSPagl shares some similar orientation and cytoarchitecture to area 30 in the primate (43–46). However, recognizing that other regions are potentially suitable for posterior midline seed regions of the default system, we ran supplementary analyses with alternative RSP candidates as well (*SI Methods* and Fig. S8).

Qualitatively comparing the DMN connections of area 30 in the macaque and humans (Fig. 6) with the RSPagl in mice (Fig. 7*A*) shows similarity in the overall pattern of connections. In the mouse, the RSPagl showed strong connectivity to the parietal, anterior cingulate, medial orbital, and parietal areas. In the human and macaque, area 30 also showed strong connectivity to the presumptive corresponding regions. Importantly, the structural connectivity of the mouse, based on the axonal tracer structural connectome, revealed similar relationships, because the functional data highlight the first-level structural–functional correspondence (Fig. 7*B*). Of note is the presence of a superior default system in humans and nonhuman primates involving area 23 in the posterior cingulate cortex (Fig. 6), a region that has no clear correlate in the mouse (40, 45) (*SI Methods*). The implication here is that, although a full DMN is not present in the mouse, an inferior subsystem is potentially conserved between species. The superior module of the default system may reflect the expansion of the cortex over time to include additional higher-order networks (40, 47, 48).

Discussion

In this report, we show on a whole-brain level the use of a robust image-processing pipeline to generate rs-fcMRI images in the mouse. We see a strong correspondence between structure and function, thus validating our procedures. We see shared, albeit not identical, connectional distributions, which highlight preserved topology across the species. Importantly, we see the presence of a default mode-like subsystem even in rodents, although as noted below, correspondence should be interpreted with care.

Structure–Function Correspondence in the Mouse Brain. Elegant studies in primates have shown concordance between functional and structural connectivity using either a combination of empirical and modeled data or the study of discrete connections using a combination of structural (projection tracing) and functional measures (fc-rsMRI) (32, 41, 49, 50). Until recently, this comparison in mice would have been limited to compiling incomplete tracer studies from individual groups, which is currently being conducted for the macaque (51). In this report, we were able to extend these studies and validate our approach by performing a whole-brain analysis in the mouse that combines mesoscale axonal projection maps with our rich functional connectivity dataset.

In agreement with the work by Shah et al. (20) and in contrast to other imaging approaches in mice, we see strong bilateral connectivity in the mouse brain, despite the use of anesthesia (52). Additionally, we also show intact distributed systems, likely because of the high-resolution imaging used combined with our innovative image acquisition and processing platform, which included directly mapping known functional areas in the mouse to the MRI data.

Although these findings were supportive of our procedures, our primary mode of validation involved the initial demonstration that, across the entire brain, functional connectivity has a strong structural foundation. As hypothesized, structural connectivity can

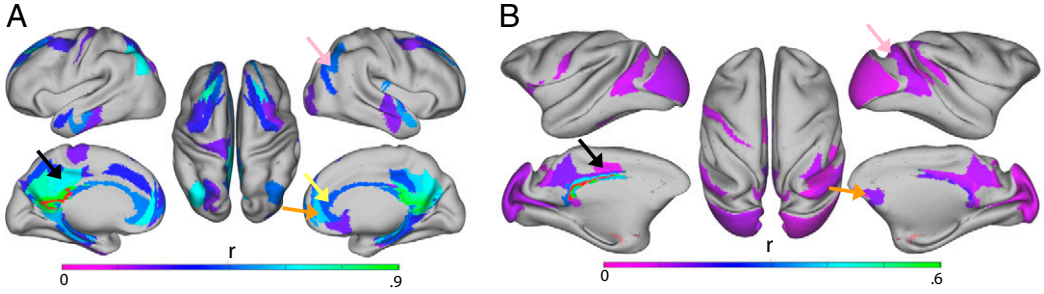

Fig. 6. The DMN in humans and macaques. Using area 30 (RSP) as the seed region (red) reveals the presence of both the inferior (DMN) subsystem and superior DMN, similar to that first described by Andrews-Hanna et al. (40, 47). The critical components of this system are the parietal cortex (pink arrow), the orbitofrontal cortex (orange arrow), and the anterior cingulate cortex (yellow arrow). Note that the superior subsystem is present in both (*A*) humans and (*B*) macaques and includes area 23 (posterior cingulate cortex; black arrow). The *r* label refers to correlation coefficient.

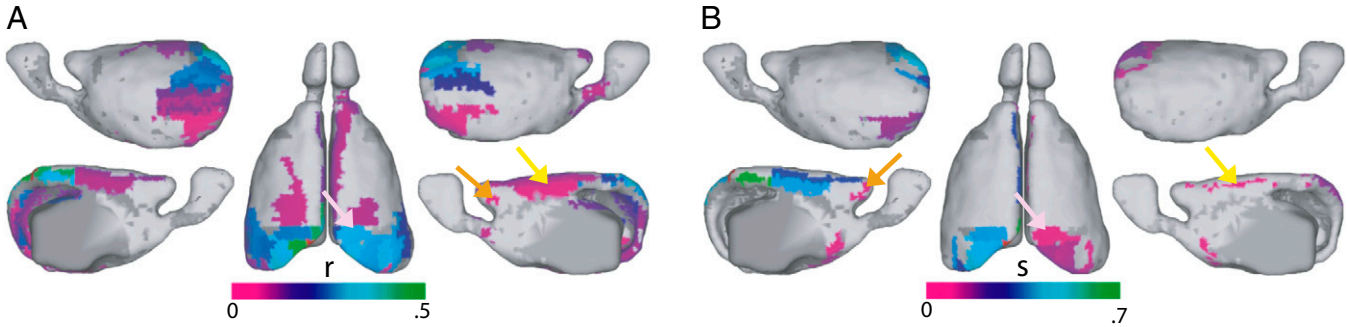

Fig. 7. Presence of the inferior DMN core in mouse functional and structural connectivity. The mouse seed region (red) used was the RSPagl, because it shows similar cytoarchitecture and location to that of area 30 in primates (45, 46). Both the (*A*) functional and (*B*) structural data in the mouse show hallmarks of the inferior DMN subsystem in primates, including the parietal cortex (pink arrow), the lateral/medial orbital cortex (orange arrow), and the cingulate area (yellow arrow). The *r* label refers to correlation coefficient; *s* refers to the relative strength of the structural connections (30).

predict functional connectivity in the mouse, a result similar to that observed on a smaller scale in humans and macaques (32–34, 41, 53–55). We note that other studies have looked at rodent functional connectivity data using rs-fcMRI with limited success (16, 19, 21, 22, 56, 57). Others have used optical intrinsic signal technique (23), which is limited to surface views of the cortex with an inability to probe deep brain structures. Here, we provide a high-resolution functional connectivity measure that overcomes a number of technical hurdles associated with imaging a small brain.

Some discrepancy between the functional and structural data was noted and could be caused by polysynaptic connections in the functional data, registration error [of the echo-planar imaging (EPI) or structural data to the atlas], signal dropout in the EPI, or other physiological confounds. Future studies optimizing the functional data acquisition, processing, and registration may lead to stronger correspondence.

Homology Between Large-Scale Functional Topology in Primates. Although some important caveats are apparent, our large-scale topological analysis provides some of the first evidence that certain properties of the functional connections between primates and mice are largely conserved; however, there were unique differences identified that may provide fodder for future study. The analysis focused on examining the way in which a node's degree (i.e., number of connections) rank dictated how it connected to the other nodes of various rank. For example, recent and prominent work in the connectivity literature has identified that the brain in primates is organized as a Rich Club. This organization seems to be an important topological feature of the primate brain but also, many other complex systems (11–13). Importantly, disruption in this level of organization has also been implicated in several complex mental disorders (58, 59). In this report, we added another level of inquiry to this particular line of work, in that we examined the nature in which highly connected nodes connect to not only the rest of the system but also, all nodes of any given rank. We felt that understanding this whole-brain topological structure provides important context in which to consider specified networks, such as the default system.

Our findings indicate that the highly connected nodes in the mouse brain (like the primate brain) are connected with each other at a rate greater than would be expected by chance (i.e., a Rich Club). These findings suggest that this topological property is conserved across the species. The findings also suggest, however, that, in humans as opposed to rodents, not only do regions that have high degree preferentially connect to nodes that also have high degrees, but nodes of any rank tended to connect to other nodes of similar rank. Such results highlight that, although the overall topology of the mouse shares features observed in primates, there are unique and likely important differences between the species with this regard.

Overall, these findings highlight that, although specific connections or putative cortical areas within the rodent and primate brain might not correspond directly across the species, many of the network properties might. Such topological features might, therefore, serve as candidates markers for cross-species translational studies (14).

Potential DMN Is Present in Mice. One of the primary goals of this report was to identify the potential presence of the DMN in mice. In a way that mimics what has previously been identified in the rat, we were, indeed, able to identify a presumptive DMN both structurally and functionally. The regions involved included cingulate, orbitofrontal, and parietal cortices both structurally and functionally. These regions overlap nicely with regions from macaques and humans (Figs. 6 and 7). Other regions in the mouse functional data were also identified that were less expected. These areas included primary visual and somatosensory areas. Although these data are consistent with work in the rat (16, 42), they do represent an important deviation from the primate brain. We note that the structural data do not show this same phenomenon, highlighting that these relationships are not monosynaptic. Nonetheless, these types of discrepancies highlight the difficulties in comparing functional connectivity patterns across primates and rodents and make clear the need for additional experimental conditions to solidify this potential homology.

Although the potential presence of this DMN subsystem appears intact in the mouse, there is a very important caveat. In primates, it has been proposed that the default system is split into a dorsal component and a more evolutionary distant ventral component (40, 48). At its core, the ventral component consists of the RSP, orbitofrontal cortex, and parietal cortices. The mouse has all of these component areas, and as noted above, they are both structurally and functionally connected (i.e., the DMN). The dorsal component of the default system consists of the posterior cingulate cortex, likely area 23 (Figs. S1–S8), and the dorsal medial prefrontal cortex at its core (40). Importantly, there is no clear correlate of area 23 in rodents (45). In addition, similarities of the frontal cortex are minimal between the rodent and humans (48). These facts suggest that, although a small component of the default system exists in the mouse, it is not present to the fullest extent as observed in primates (Figs. 6 and 7).

We note that examining DMN homology between species should be interpreted with care considering the difficulty in precisely linking corresponding areas between species. Nonetheless, the findings presented here suggest that a subcomponent of the DMN is present in the mouse, enabling the use of high-throughput genetic, histological, and therapeutic manipulations that can be applied to better understand the system's function in health and disease.

Methods

Detailed methods are described in *SI Methods*. In total, nine C57Bl/6J adult male mice were used in the rs-fcMRI experiments. All mice were anesthetized with 1–1.5% (vol/vol) isoflurane throughout the MRI procedure. All Human Subjects provided written consent for the imaging protocols approved by the Oregon Health & Science University Institutional Review Board (IRB).

For rs-fcMRI, a Bruker 11.75T magnet equipped with a high-bandwidth shim power supply and MAPSHIM automated shimming was used to maximize resolution and improve local field homogeneity. The rs-fcMRI consisted of a single-shot gradient EPI sequence. After acquisition, distortion was further decreased, and signal to noise was improved with a number of processing techniques frequently used in human fc-MRI studies (*SI Methods*).

From resting-state blood oxygen level-dependent data, separate region of interest resting time series were extracted separately and correlated region by region for each animal to create correlation matrices (represented as *r* in each color bar). Structural data were obtained from the Allen Institute for Brain Science. Both qualitative and quantitative analyses were carried out as detailed in *SI Methods*.

ACKNOWLEDGMENTS. We thank Lydia Ng of the Allen Institute for Brain Sciences for providing scripts for extracting raw data from the structural connectome database. We also thank David Grayson, Andrew Woodall, Kathleen A. Grant, and Christopher D. Kroenke for critical discussions and help with analysis. Funding was provided by OHSU Clinical and Translational Research Institute Grants UL1TR000128 (to J.T.N. and D.A.F.), R01MH096773 (to D.A.F.), and R00MH091238 (to D.A.F.). Support for J.M.S. was from Grants F31MH087031 and F32AA022842 and as a Simons Foundation Junior Fellow.

1. Logothetis NK (2012) Intracortical recordings and fMRI: An attempt to study operational modules and networks simultaneously. *Neuroimage* 62(2):962–969.
2. Fair DA, et al. (2008) The maturing architecture of the brain's default network. *Proc Natl Acad Sci USA* 105(10):4028–4032.
3. Hagmann P, et al. (2010) White matter maturation reshapes structural connectivity in the late developing human brain. *Proc Natl Acad Sci USA* 107(44):19067–19072.
4. Grayson DS, et al. (2014) Structural and functional rich club organization of the brain in children and adults. *PLoS ONE* 9(2):e88297.
5. Di Martino A, et al. (2014) Detection of functional connectivity in the resting mouse brain. *Neuroimage* 86:417–424.
6. Seeley WW, Crawford RK, Zhou J, Miller BL, Greicius MD (2009) Neurodegenerative diseases target large-scale human brain networks. *Neuron* 62(1):42–52.
7. Fair DA, et al. (2010) Atypical default network connectivity in youth with attention-deficit/hyperactivity disorder. *Biol Psychiatry* 68(12):1084–1091.
8. Douaud G, et al. (2007) Anatomically related grey and white matter abnormalities in adolescent-onset schizophrenia. *Brain* 130(Pt 9):2375–2386.
9. Vincent JL, et al. (2007) Intrinsic functional architecture in the anaesthetized monkey brain. *Nature* 447(7140):83–86.
10. Biswal B, Yetkin FZ, Haughton VM, Hyde JS (1995) Functional connectivity in the motor cortex of resting human brain using echo-planar MRI. *Magn Reson Med* 34(4):537–541.
11. Colizza V, Flammini A, Serrano MA, Vespignani A (2006) Detecting rich-club ordering in complex networks. *Nat Phys* 2(2):110–115.
12. van den Heuvel MP, Sporns O (2011) Rich-club organization of the human connectome. *J Neurosci* 31(44):15775–15786.
13. Zhou S, Mondragon RJ (2004) The rich-club phenomenon in the internet topology. *IEEE Commun Lett* 8:180–182.
14. Miranda-Dominguez O, et al. (2014) Bridging the gap between the human and macaque connectome: A quantitative comparison of global interspecies structure-function relationships and network topology. *J Neurosci* 34(16):5552–5563.
15. Hutchinson E, et al. (2010) Children with new-onset epilepsy exhibit diffusion abnormalities in cerebral white matter in the absence of volumetric differences. *Epilepsy Res* 88(2-3):208–214.
16. Lu H, et al. (2012) Rat brains also have a default mode network. *Proc Natl Acad Sci USA* 109(10):3979–3984.
17. Pawela CP, et al. (2008) Resting-state functional connectivity of the rat brain. *Magn Reson Med* 59(5):1021–1029.
18. Shim WH, et al. (2013) Frequency distribution of causal connectivity in rat sensorimotor network: Resting-state fMRI analyses. *J Neurophysiol* 109(1):238–248.
19. van Meer MP, et al. (2010) Recovery of sensorimotor function after experimental stroke correlates with restoration of resting-state interhemispheric functional connectivity. *J Neurosci* 30(11):3964–3972.
20. Shah D, et al. (2013) Resting state FMRI reveals diminished functional connectivity in a mouse model of amyloidosis. *PLoS ONE* 8(12):e84241.
21. Little DM, Foxely S, Lazarov O (2012) A preliminary study targeting neuronal pathways activated following environmental enrichment by resting state functional magnetic resonance imaging. *J Alzheimers Dis* 32(1):101–107.
22. Nasrallah FA, Tay HC, Chuang KH (2014) Detection of functional connectivity in the resting mouse brain. *Neuroimage* 86:417–424.
23. White BR, et al. (2011) Imaging of functional connectivity in the mouse brain. *PLoS ONE* 6(1):e16322.
24. Mechling AE, et al. (2014) Fine-grained mapping of mouse brain functional connectivity with resting-state fMRI. *Neuroimage* 96:203–215.
25. Raichle ME, et al. (2001) A default mode of brain function. *Proc Natl Acad Sci USA* 98(2):676–682.
26. Shulman GL, et al. (1997) Common blood flow changes across visual tasks: II. Decreases in cerebral cortex. *J Cogn Neurosci* 9(5):648–663.
27. Greicius MD, Srivastava G, Reiss AL, Menon V (2004) Default-mode network activity distinguishes Alzheimer's disease from healthy aging: Evidence from functional MRI. *Proc Natl Acad Sci USA* 101(13):4637–4642.
28. Grayson DS, Kroenke CD, Neuringer M, Fair DA (2014) Dietary omega-3 fatty acids modulate large-scale systems organization in the rhesus macaque brain. *J Neurosci* 34(6):2065–2074.
29. Broyd SJ, et al. (2009) Default-mode brain dysfunction in mental disorders: A systematic review. *Neurosci Biobehav Rev* 33(3):279–296.
30. Oh SW, et al. (2014) A mesoscale connectome of the mouse brain. *Nature* 508(7495):207–214.
31. Hagmann P, et al. (2008) Mapping the structural core of human cerebral cortex. *PLoS Biol* 6(7):e159.
32. Honey CJ, Kötter R, Breakspear M, Sporns O (2007) Network structure of cerebral cortex shapes functional connectivity on multiple time scales. *Proc Natl Acad Sci USA* 104(24):10240–10245.
33. Honey CJ, et al. (2009) Predicting human resting-state functional connectivity from structural connectivity. *Proc Natl Acad Sci USA* 106(6):2035–2040.
34. van den Heuvel MP, Mandl RC, Kahn RS, Hulshoff Pol HE (2009) Functionally linked resting-state networks reflect the underlying structural connectivity architecture of the human brain. *Hum Brain Mapp* 30(10):3127–3141.
35. Loudin JD, Miettinen HE (2003) A multivariate method for comparing n-dimensional distributions. *Proceedings of the Conference on Statistical Problems in Particle Physics, Astrophysics and Cosmology (PHYSTAT)*, eds Lyons L, Mount R, Reitmeyer R (PHYSTAT, Stanford, CA), pp 207–210.
36. Towlson EK, Vértes PE, Ahnert SE, Schafer WR, Bullmore ET (2013) The rich club of the C. elegans neuronal connectome. *J Neurosci* 33(15):6380–6387.
37. van den Heuvel MP, Sporns O (2013) Network hubs in the human brain. *Trends Cogn Sci* 17(12):683–696.
38. Paxinos G, Huang XF, Toga A (1999) *The Rhesus Monkey Brain in Stereotaxic Coordinates. Faculty of Health and Behavioural Sciences—Papers* (Archive, San Diego).
39. Van Essen DC (2005) Surface-based comparisons of macaque and human cortical organization. *From Monkey Brain to Human Brain. A Fyssen Foundation Symposium*, ed Dehane S (MIT Press, Cambridge, MA), pp 3–20.
40. Andrews-Hanna JR, Reidler JS, Sepulcre J, Poulin R, Buckner RL (2010) Functional-anatomic fractionation of the brain's default network. *Neuron* 65(4):550–562.
41. Greicius MD, Supekar K, Menon V, Dougherty RF (2009) Resting-state functional connectivity reflects structural connectivity in the default mode network. *Cereb Cortex* 19(1):72–78.
42. Upadhyay J, et al. (2011) Default-mode-like network activation in awake rodents. *PLoS ONE* 6(11):e27839.
43. Kobayashi Y, Amaral DG (2003) Macaque monkey retrosplenial cortex: II. Cortical afferents. *J Comp Neurol* 466(1):48–79.
44. Morris R, Petrides M, Pandya DN (1999) Architecture and connections of retrosplenial area 30 in the rhesus monkey (Macaca mulatta). *Eur J Neurosci* 11(7):2506–2518.
45. Vogt BA, Vogt L, Farber NB (2004) Cingulate cortex and disease models. *The Rat Nervous System*, ed Paxions G (Academic, Waltham, MA), 3rd Ed, pp 705–727.
46. Vogt BA, Paxinos G (2014) Cytoarchitecture of mouse and rat cingulate cortex with human homologies. *Brain Struct Funct* 219(1):185–192.
47. Andrews-Hanna JR, Reidler JS, Huang C, Buckner RL (2010) Evidence for the default network's role in spontaneous cognition. *J Neurophysiol* 104(1):322–335.
48. Buckner RL, Krienen FM (2013) The evolution of distributed association networks in the human brain. *Trends Cogn Sci* 17(12):648–665.
49. Sallet J, et al. (2013) The organization of dorsal frontal cortex in humans and macaques. *J Neurosci* 33(30):12255–12274.
50. Wang Z, et al. (2013) The relationship of anatomical and functional connectivity to resting-state connectivity in primate somatosensory cortex. *Neuron* 78(6):1116–1126.
51. Stephan KE (2013) The history of CoCoMac. *Neuroimage* 80:46–52.
52. Jonckers E, Van Audekerke J, De Visscher G, Van der Linden A, Verhoye M (2011) Functional connectivity fMRI of the rodent brain: Comparison of functional connectivity networks in rat and mouse. *PLoS ONE* 6(4):e18876.
53. Koch MA, Norris DG, Hund-Georgiadis M (2002) An investigation of functional and anatomical connectivity using magnetic resonance imaging. *Neuroimage* 16(1):241–250.
54. Schölvinck ML, Maier A, Ye FQ, Duyn JH, Leopold DA (2010) Neural basis of global resting-state fMRI activity. *Proc Natl Acad Sci USA* 107(22):10238–10243.
55. van den Heuvel M, Mandl R, Luigjes J, Hulshoff Pol H (2008) Microstructural organization of the cingulum tract and the level of default mode functional connectivity. *J Neurosci* 28(43):10844–10851.
56. Pawela CP, et al. (2009) A protocol for use of medetomidine anesthesia in rats for extended studies using task-induced BOLD contrast and resting-state functional connectivity. *Neuroimage* 46(4):1137–1147.
57. Pawela CP, et al. (2008) Modeling of region-specific fMRI BOLD neurovascular response functions in rat brain reveals residual differences that correlate with the differences in regional evoked potentials. *Neuroimage* 41(2):525–534.
58. van den Heuvel MP, et al. (2013) Abnormal rich club organization and functional brain dynamics in schizophrenia. *JAMA Psychiatry* 70(8):783–792.
59. Ray S, et al. (2014) Structural and functional connectivity of the human brain in autism spectrum disorders and attention-deficit/hyperactivity disorder: A rich club-organization study. *Hum Brain Mapp* 35(12):6032–6048.